Interfacial Water-Transport Effects in Proton-Exchange Membranes

Brian Kientiz,[1] Haruhiko Yamada,[2] Nobuaki Nonoyama,[3] and Adam Z. Weber[1,*]

[1]Environmental Energy Technologies Division, Lawrence Berkeley National Laboratory, Berkeley, CA 94720, USA.

[2]Toyota Central R&D Labs, Inc, Nagakute, Aichi, 480-1192, Japan

[3]Higashifuji Technical Center, Toyota Motor Corporation, Susono, Shizuoka, 410-1193, Japan

It is well known that the proton-exchange membrane is perhaps the most critical component of a polymer-electrolyte fuel cell. Typical membranes, such as Nafion®, require hydration to conduct efficiently and are instrumental in cell water management. Recently, evidence has been shown that these membranes might have different interfacial morphology and transport properties than in the bulk. In this paper, experimental data combined with theoretical simulations will be presented that explore the existence and impact of interfacial resistance on water transport for Nafion® 21x membranes. A mass-transfer coefficient for the interfacial resistance is calculated from experimental data using different permeation cells. This coefficient is shown to depend exponentially on relative humidity or water activity. The interfacial resistance does not seem to exist for liquid/membrane or membrane/membrane interfaces. The effect of the interfacial resistance is to flatten the water-content profiles within the membrane during operation. Under typical operating conditions, the resistance is on par with the water-transport resistance of the bulk membrane. Thus, the interfacial resistance can be dominant especially in thin, dry membranes and can affect overall fuel-cell performance.

Keywords: Polymer-electrolyte fuel cell; water transport; proton-exchange membrane; interfacial resistance

*Corresponding author, phone: 510-486-6308, fax: 510-486-7303, email: azweber@lbl.gov

Introduction

Perfluorosulfonic-acid (PFSA) based polymer-electrolyte fuel cells (PEFC) are an attractive alternative energy technology due to their low point-source emissions and ability to use renewably-derived fuels. The proton-exchange membrane in a PEFC must serve many functions within the cell. It must be conductive to protons while resistive to electrons, provide a gas barrier between the anode and cathode, and be durable enough to operate under harsh PEFC conditions for thousands of hours. Proper water management inside the membrane is paramount to the function of a PEFC. Low water content in the membrane increases the ohmic losses in the fuel cell. On the other hand, too much water can lead to flooding of the catalyst and gas-diffusion layers. Both of these cases reduce PEFC system performance. Therefore, a thorough understanding of how water is transported in membranes is needed to design, model, and optimize water management – and therefore cell performance - in PEFC systems.

Water is transported across a membrane by a chemical-potential gradient that can be attributed to pressure gradients or concentration gradients. The resistance to and transport of water in the bulk of the membrane have been modeled in accordance with physical transport laws [1]. Membranes in PEFCs have trended thinner to reduce the ohmic losses and increase water transport across the cell; however, as the membranes used become thinner (now on the order of tens of microns), transport at and through membrane interfaces can result in significant transport resistances that cannot necessarily be characterized by bulk membrane properties. Finally, these interfaces are expected to occur throughout the catalyst layer, making the ionomer there possess different transport properties.

Zawodzinski *et al* showed that the contact angle at the surface of Nafion® membranes (a common membrane used in PEFCs) changed from hydrophilic to hydrophobic as the membrane dried [2]. They hypothesized that this effect might be caused by the formation of a hydrophobic skin at the surface of Nafion® membranes. Removing this surface by sputter etching with argon increased PEFC performance [3]. The presence of a hydrophobic surface was further confirmed using conducting atomic-force microscopy [4-7]. It has also been qualitatively demonstrated that membrane surfaces are more hydrophobic at lower relative humidities. Van Nguyen and coworkers showed that there is a large difference in conductive surface area between membranes equilibrated at 30 and 80% relative humidity [7]. Aleksandrova *et al* have demonstrated that the relative humidity can affect the percentage of surface area that shows conductivity and that this increase is linear between 40 and 50% relative humidity [5]. Likely, the change in hydrophobicity affects both conductivity and water transport across the membrane surface.

Several papers have attempted to measure and calculate the interfacial and bulk water-transport properties of proton-exchange membranes [8-13]. Others have also tried to measure other transport properties of the system such as conductivity [14] and gas transport [15] in similar manners. In general, water transport across membranes has been measured by applying a water-activity gradient across the membrane. This is usually accomplished by exposing one side of the membrane to liquid water or saturated vapor and exposing the other side to a dry gas stream. The water exiting with the dry gas stream is collected and measured to quantify the water flux across the membrane. Others have measured the sorption of water over time [8-11, 13, 16-18]. The measured water fluxes have not been consistent in the literature. Majsztrik *et al* provides a good summary of different diffusion coefficients determined by these methods [13]. These differences are likely due to differences in experimental apparatus and techniques,

differences in determination of the coefficients (whether interfacial resistances were considered or not), and inaccuracies due to a limited number of data points. For instance, water flux is often measured as a function of membrane thickness, but relatively few Nafion thicknesses are commercially available. One of the most thorough studies of water transport rates in Nafion® 21x membranes is done by Adachi *et al*. [16]. They measured different transport coefficients depending on whether the membrane had liquid or vapor in contact with it. However, while they witnessed different transport rates for the different arrangements, and an apparent offset with vapor boundaries, they did not explore and quantify the interfacial impacts in detail.

The interfacial resistances calculated in the literature have varied by at least an order of magnitude. This is partially due to the inaccuracy of the measurement techniques, but also significantly due to the differences in which the data has been analyzed. For instance, some papers have shown evidence that the interfacial resistance dominates the water transport [10, 13], while others have shown that bulk-diffusion dominates the resistance [12] . Obviously the relative importance of the interface is dependent on membrane thickness, but it also is likely dependent on water activity. New experimental evidence must be collected and models developed to capture fully these effects. One of the largest problems in analyzing data from water-transport experiments is that the membrane properties can change drastically as a function of membranes water content [19-23].

In a working PEFC, the membrane can be exposed to a large range of water conditions: near the anode feed inlet it can be almost completely dry if non-humidified gases are used, and, in contrast, water formation at the cathode results in much higher humidities and even liquid water there. The membrane water activity may be anywhere in between these extremes. It is likely that the interfacial resistance is a function of the water activity present at the interface just

like the water transport coefficient and other properties, where drier interfaces may lead to higher interfacial resistances in accordance with an expected lower amount of surface hydrophilic moieties as mentioned above. To our knowledge no one has tried to correlate and model the interfacial resistance as a function of the water activity at the surface of a Nafion membrane. In this paper we create an experimental and theoretical framework to measure this relationship and show how it can affect water management in a PEFC.

This paper is broken into three parts. First, the experimental and theoretical procedures are described. Second, the data for the water transport properties and interfacial resistance are detailed with respect to the permeation-cell setup for Nafion® 21x membranes. Finally, the third part contains some detailed simulation results for water-content profiles and impacts related to current flow, followed by a summary and future directions to be explored.

Experimental and Theory

Permeation measurements

A cell was designed that could measure the permeation of water due to a liquid-water pressure gradient across Nafion®. A schematic of this cell can be seen in Figure 1a. Two chambers were separated by a Nafion® NRE 212 or 211 membrane and filled with water. Each chamber had one port. The port on the first chamber was used to pressurize the water in the chamber. The port on the second chamber was used to keep that chamber at atmospheric pressure and to measure the amount of water that had permeated across the membrane. A highly

porous metal support (CELMET, Sumitomo Electric Toyama) was used to brace the membrane on the side of lower pressure to keep the membrane from bending and tearing.

The flux of water across the membrane was calculated from the total amount of water transported across the membrane over time. Absolute permeabilities (k_{sat}) were calculated from the water-flux data and are defined as

$$k_{sat} = \frac{\mu \mathbf{N} \bar{V}_w t}{\Delta p} \quad [1]$$

where **N** is the water flux, μ is the water viscosity at the temperature investigated, Δp is the liquid-pressure difference, t is the membrane thickness, and $\bar{V}_w$ is the molar volume of water. Data were collected for Nafion® 212 membranes at temperatures of 25, 60 and 80°C and for Nafion 211 membranes at 25°C. Measurements at each condition were repeated three times.

A second permeation cell was created to measure the flux of water across Nafion® membranes subject to an activity gradient by equilibrating one (LE/VE) or two sides (VE/VE) of the membrane with water vapor as shown in Figure 1b. The cell once again consisted of a Nafion® membrane separating two chambers. In this cell, each chamber contained both an inlet and outlet port so that gases could flow through the chamber and a membrane support was not necessarily required although the highly porous metal supports could be added or removed from both sides of the membrane. For the LE/VE case, a slightly different cell was used where these ports were not used and the chamber was simply filled with water. Gas flow meters (MC-3102E-NC, LINTEK) were used to regulate the flow in the VE chambers. The gas used for LE/VE experiments was air, and that for VE/VE experiments was hydrogen. Relative humidity of the inlet gas was controlled by mixing dry and humidified streams.

Humidity sensors (Chilled-mirror hygrometer SIM-12H, GENERAL EASTERN) were placed on the gas inlet and outlet of the two chambers. The difference in humidity between the inlet and outlet gas along with the gas flow rate was used to determine the water flux across the membrane. The activity of the membrane interface exposed to the second chamber was calculated as the log-mean average between the inlet and outlet activities. The activity gradient across the cell was then used to calculate diffusion coefficients and interfacial resistances discussed in the modeling section.

Two sets of experiments were performed with this setup. In the first set, one chamber was held at a constant relative humidity of 100%. The relative humidity of the second chamber was varied from 20% to 80% as in typical flow experiments. In the second set, the average relative humidity in the membrane was varied and the difference between the two chambers was held at less than 10% relative humidity (i.e., a differential experiment). In this way, the two interfacial resistances could be averaged to determine a value for the interfacial resistance corresponding to the average membrane relative humidity.

Mathematical Modeling

Experimental data were fit to a model to derive interfacial and bulk membrane transport properties. The model is an extension of the water-transport model developed by Weber and Newman[19, 24]. The model utilizes a chemical-potential gradient for water transport

$$\mathbf{N} = -\alpha \nabla \mu_{w} \qquad [2]$$

where the above gradient can be written as

$$\nabla \mu_{w} = RT \nabla \ln a + \bar{V}_{w} \nabla p = RT \nabla \ln(\mathrm{RH}) + \bar{V}_{w} \nabla p \qquad [3]$$

where RH is the relative humidity of the gas, $\overline{V}_w$ is the partial molar volume of water, and a secondary reference state of saturated gas is taken. In equation 2, α is a transport coefficient that is a function of water content (λ or moles of water per mole of sulfonic acid site) and the state of the membrane (liquid or vapor-equilibrated)

$$\alpha = \alpha_L S + (1-S)\alpha_V = \frac{k_{sat}}{\mu \overline{V}_w^2} S + (1-S)\frac{c_w D_\mu}{RT(1-x_w)} \quad [4]$$

where R is the ideal gas constant, T is the absolute temperature, c_w and x_w are the concentration and mole fraction of water, respectively, D_μ is the diffusion coefficient of water related to the chemical-potential driving force, and S is related to the chemical potential of any liquid water. From previous data, D_μ is a function of temperature and water content[19]

$$D_\mu = 1.8\times10^{-5}\lambda \exp\left[\frac{20000}{R}\left(\frac{1}{T_{ref}} - \frac{1}{T}\right)\right] \quad [5]$$

For a membrane that is only vapor-equilibrated, one can rewrite the vapor-equilibrated transport coefficient (equation 4) as

$$\alpha_V = \frac{D_\mu}{RT}\frac{\lambda(\lambda+1)\overline{V}_w}{\overline{V}_m} \quad [6]$$

To determine the water content, λ, two equations are solved from a thermodynamically consistent Gibbs function, which is fit to the measured isopiestic curves [19]. Finally, swelling of Nafion 21x membranes was measured at liquid equilibration, giving an expression for the membrane thickness of

$$t = t_o\left(1 + 0.083\frac{\hat{\lambda}\,\overline{V}_w}{\overline{V}_m}\right) \quad [7]$$

where t_o is the dry thickness, $\overline{V}_m$ is the partial molar volume of membrane, and $\hat{\lambda}$ is the average membrane water content, which is solved for.

For the simulations with current flowing, the governing transport equations from concentrated solution theory are

$$\mathbf{i} = -\kappa\nabla\Phi - \frac{\kappa\xi}{F}\nabla\mu_w \quad [8]$$

and

$$\mathbf{N} = -\frac{\kappa\xi}{F}\nabla\Phi - \left(\alpha + \frac{\kappa\xi^2}{F^2}\right)\nabla\mu_w \quad [9]$$

where **i** is the current density, Φ is the ionic potential, ξ is the electro-osmotic coefficient, F is Faraday's constant, and κ is the conductivity. Both κ and ξ are functions of water content and temperature [19]. For thermal transport, thermal conduction is considered

$$\mathbf{q} = -k_T\nabla T \quad [10]$$

where **q** is the heat flux and k_T is effective membrane thermal conductivity.

In addition to the transport equations above, conservation equations at steady state are applied

$$\nabla\cdot\mathbf{i} = 0 \quad [11]$$

$$\nabla\cdot\mathbf{N} = 0 \quad [12]$$

and

$$\nabla \cdot \mathbf{q} = \frac{\mathbf{i}^2}{\kappa} \qquad [13]$$

where the last term in equation 13 represents ohmic heating. The boundary conditions applied are a chemical potential at each side, a zero potential reference, the current density, and a constant temperature on the membrane boundaries.

In this paper, the above model has been expanded to employ new experimental data and include interfacial effects. These interfacial effects are included in the chemical-potential boundary conditions of the governing equations. In essence, the water activity at the boundary is adjusted to account for the transport resistance through a small interfacial boundary whenever the boundary is exposed to water in the vapor form. At steady state the flux through the boundary must be equal to the flux through the rest of the membrane. It is assumed that the flux through the boundary is proportional to a change in water activity across the boundary

$$N = k\left(a_{\text{in}} - a_{\text{out}}\right) \qquad [14]$$

where in and out refer to the water activities directly inside and outside of the membrane interface and k is a mass-transfer coefficient.

The boundary acts as a resistance in series along with the resistance across the bulk of the membrane

$$N = \frac{\Delta a}{R} = \frac{\Delta a}{\frac{t}{\alpha} + \frac{1}{2k}} \qquad [15]$$

where the factor of two is due to the exposure of both membrane sides to vapor. The slope of equation 15 as a function of membrane thickness is inversely proportional to the water transport

coefficient in the membrane. The non-zero intercept is inversely proportional to the mass-transfer coefficient across the membrane interface.

Results and discussion

Liquid-equilibrated/liquid-equilibrated system

Water permeation experiments were carried out for liquid-equilibrated (LE) membranes where a pressure gradient of liquid water was forced across the cell. A permeability was fit to this data through a least squares fit of equation 1. Table I shows how the permeability changes as a function of cell temperature and thickness. The permeability itself is a function of temperature, besides the already accounted for impact of viscosity changes with temperature. Increasing temperature from 25 to 80°C resulted in a six-fold increase in permeability. The permeability of water across Nafion® membranes, as measured in this paper, is small compared to values previously measured [25], although those values were measured for extruded Nafion 1100 membranes. It is likely that the Nafion® 21x membranes have a much lower liquid permeability due to their structure. Furthermore, the value found here is only slightly below that measured recently by Adachi *et al.*[16], which could be explained by some small pressure drop related to the reinforcing mesh. It is likely that the importance of pressure-driven flow in PEFC systems is less in Nafion® 212 and 211 membranes than in Nafion® 1100 series membranes.

The permeability was also determined for two sets of Nafion® 21x membranes with different thicknesses. The permeability for the two sets of membranes was 1.09×10^{-16} cm^2 for both membranes with deviations of less than 0.05×10^{-16} for both thicknesses (see Table I). This

data corroborates the hypothesis that there is no additional interfacial resistance to liquid-water flow across Nafion® membranes and that the interfaces can be treated the same as the bulk of the membrane when the interface is LE. As discussed later, this data reinforces the idea that the hydrophobic layer that forms on Nafion® membranes when they are VE is the main cause of interfacial resistances to water transport. It is of interest to note that an interfacial effect on the conductivity of Nafion® membranes has been seen even when the membranes were fully submerged in water [14]. Therefore it is probable that interfacial resistance to water transport and proton transport across Nafion® membranes is not exclusively due to the same mechanism.

Liquid-equilibrated/Vapor-equilibrated system

Figure 2 shows the water flux across a LE/VE cell with a Nafion® 212 membrane as a function of liquid-water pressure in the first chamber for different relative-humidity gas streams in the second chamber at 80°C. The water flux increases as the relative-humidity difference between the inlet gases in chambers one and two is increases from between a value of 20 to that of 60%. The decreases seem somewhat proportional to the activity gradient, although no clear functional dependence can be derived since flux data for only three water activities were measured.

The significantly lower water permeability as measured using the LE/LE permeation cell is evident in the LE/VE data where the flux is nearly constant as liquid pressure is increased. As the pressure gradient is increased from 0 to 300 kPa the increase in water transport is nearly negligible. In this case, transport due to differences in relative humidity across the cell greatly outweighs any flux due to pressure gradients across the cell. This is in agreement with the findings of Adachi *et al*. who witnessed larger fluxes due to the larger chemical-potential

gradient in the LE/VE system more than offsetting the difference in transport coefficients [16]. Therefore, one could, to a good approximation, neglect pressure-driven flow across these membranes in models as long as there was also an activity-gradient driven flow.

Vapor-equilibrated/Vapor-equilibrated system

Water-flux data were collected for small RH differences (less than 10%) across Nafion 21x membranes of different thicknesses. This data is shown in Table II. Flux data was normalized by the activity gradient across the cell and inverted to calculate a transport resistance (see equation 12). The resistance values are plotted in Figure 3 as a function of membrane wet thickness for different levels of activities (Figure 5 plots the actual fluxes). The resistance values can be compared to those in the literature by multiplying them by the molar density of water in the membrane to yield a resistance in units of s/cm. From the data, one can also see that the membrane/membrane interface does not provide any resistance to water transport, which is in agreement with the data for the LE/LE and VE/VE cases with multiple membranes (not shown). The slope of the resistance lines is related to the diffusion coefficient and the intercepts at zero thickness are interpreted as the interfacial resistance.

From the experimental data, an effective interfacial resistance as a function of water activity can be calculated by assuming the simple relationship in equation 15. The derived interfacial resistance coefficient as a function of water activity is shown in Figure 4. An exponential curve fit has been derived from this data to assist in modeling

$$k = 1.04\times10^{-7}\,\mathrm{e}^{4.48\times10^{-4}a}\ \frac{\mathrm{mol}}{\mathrm{cm}^2\mathrm{s}} \qquad [16]$$

As further validation, the above relationship was added to the boundary condition for water chemical potential, and the fluxes for the VE/VE system calculated. Figure 5 shows a comparison between the modeled normalized flux data and the experimental results. As seen, the agreement between the two is good, lending credence to both the modeling approach and the derived values. Also, the result of the interfacial resistance being a function of relative humidity is in accordance with the work of others as noted in the introduction.

The diffusion coefficient calculated from these experiments agrees closely with other measurements [9, 23, 26, 27]. From the data, values at 100% RH and 80°C of between 2.5×10^{-5} and 3.25×10^{-5} cm^2/s are calculated, which compares favorably with the value of 2.7×10^{-5} cm^2/s from equation 5. Membrane thickness is also shown to have little effect on the internal diffusion coefficient, as expected. The values reported here are larger than those of Adachi *et al*., although they did not account for the interfacial resistance (i.e., their transport coefficients contain both the resistance due to the bulk and the interface) [16].

From the simulation results, one can calculate the relative contributions of the interface and bulk towards the overall resistance to water flow. Figure 6 displays the fraction of total resistance due to interfacial effects as a function of both membrane thickness and water activity. Figure 6 demonstrates two trends. First, interfacial resistance becomes more important as membrane thickness decreases, which is not surprising since as the membrane thickness approaches zero the membrane is in essence "all interface." Second, the figure shows the effect that drier interfaces have on the interfacial resistance. When the water activity is decreased from 0.85 to 0.25 the fraction of total resistance due to the interface doubles. For thin, dry membranes the interface can easily become more important than the bulk properties. Even typical membranes used in PEFCs at typical conditions (e.g., 25.4 microns at 80% relative humidity)

show significant interfacial effects. These results are consistent with those of Monroe *et al*. [10] and Benziger and coworkers [11, 28] and underscore the importance of accounting for membrane interfacial resistance in analyzing and modeling PEFC behavior.

Finally, some data were taken (not shown) to compare the LE/VE and VE/VE cases where one side is at 100% RH. These data used a mesh, which had an unknown mass-transfer resistance; however, qualitatively they show that there is an extra resistance with the 100% VE than with LE, in agreement with the data of Adachi *et al*.[16] and the above analysis.

Simulations

The above-described interfacial resistances and lower water permeability both affect the water-content profile across the membrane. Most models set boundary conditions of chemical potentials, activities, or associated equilibrium water-content values. The interfacial resistance lowers the chemical potential at the interfaces because there is a change in chemical potential across the interface. This interface is modeled as being infinitely small (see equation 14). To explore the impact of the permeability and interfacial resistance on the water content, different cases were run and their profiles compared in Figure 7. The two VE/VE cases show the effect of the interfacial resistance on the water-content profile. The gradient in the profile is smaller for the case with interfaces even though the water activity at the boundary is the same for both cases. The two LE/VE cases show the effect of the lower permeability of water on the profile. In membranes with lower water permeability, like Nafion® 21x membranes, the membrane becomes VE very near the LE side. This is not necessarily the case of the LE/VE case with higher permeability.

The interfacial effects with current passage were also investigated with the model. Since this is a membrane-only model and focusing on water transport, other cell components and operating conditions such as gas flow rate, diffusion media, and catalyst layers are ignored. To be general, two extreme cases that encompass most of the membrane operating conditions are used. These cases are characterized by the boundary condition at the interface between the membrane and low-activity gas. Using a Dirichlet boundary condition at this interface approximates the case where there is abundant gas flow and the membrane activity is in equilibrium with the gas stream. A Neumann boundary condition sets the water flux into the membrane, which approximates the case where gas flow is close to the stoichiometric proportion and water flux is limited by the amount of water entering from the inlet gas stream. In all cases the high activity side is set to be at 100% relative humidity.

Current density changes water content in the membrane due to the electro-osmotic flux caused as protons carry water while flowing across the membrane (see equations 8 and 9). It is assumed that the electro-osmotic coefficient is not affected by the interface. If this assumption is valid then the water content in the membrane is not affected by current directly for the Dirichlet boundary condition. In this case, the activity loss through the interface is determined by the gradient flux through the membrane. A temperature increases in the membrane as current increases can affect the back diffusion, thus affecting the activity loss at the interface; these effects are of secondary importance.

In the second case, where a Neumann boundary condition is used, the water content of the membrane is a function of current density. In this case, the flux due to diffusion and the flux due to electro-osmosis must always add to a constant (see equation 12). Figure 8 shows the water activity at the low-humidity side as a function of current density across the membrane for

three different net water fluxes. For comparison, the corresponding curve for the case of zero interfacial resistance is also included for each water flux.

When the net water flux is less than zero, back diffusion is greater than electro-osmosis. In this case, the activity of water at the gas/membrane interface is lower than unity. This activity difference is the driving force for transport. When the water flux is set to zero, the back diffusion and electro-osmosis are equal. At zero current, there is no electro-osmosis (streaming current is minimal), and the water activity at the gas/membrane interface is unity. When the water flux is positive, electro-osmosis is larger than the back diffusion. In this case, the curve does not exist at currents lower than the current required to produce sufficient electro-osmotic flux.

For each case described above, the water activity at the anode gas/membrane interface decreases as the current increases. This decrease is because a larger activity gradient is needed to counter the increased electro-osmotic flux. The water activity reaches zero at the gas/membrane interface at lower currents when interfacial effects are included. This effect is only significant when the membrane is dry. The difference between the curves correlates to the fraction of resistance due to the interface as shown in Figure 6. At low water activities, the interface accounts for 20 to 30% of the total activity gradient.

The decrease in water activity can be interpreted two ways. First, the interface leads to anode dry out at lower current densities than systems without an interface. This will cause performance problems, especially with low relative-humidity gas streams. Second, and conversely, the water activity directly inside the anode of an operating PEFC will have a water activity greater than the gas feed stream water activity. This will increase the conductivity of the

membrane near the anode even when little water is available. This effect will likely be counteracted by a decrease in the conductance of the interface. Since the resistance of the interface to ion transport is not well understood, it is impossible to know which effect would dominate in this case. Still, increasing PEFC performance by engineering the gas/membrane interface may be a plausible way to reducing the need for fully hydrated feed streams. An interesting exploration would be to determine whether the water produced in the catalyst layer is in the membrane or outside of it, since this would impact whether the gas or membrane contained the higher water activity. In addition, the catalyst-layer ionomer is not well understood and could even be all interface with significant impacts on gas, water, and proton transport; more research is necessary.

Summary

In this paper the permeability of liquid water for Nafion® 21x membranes was determined, and is lower than that found in older, esxtruded Nafion. In addition, the transport of water vapor across membranes was presented and discussed. It was determined that there is an interfacial resistance, which is described by a mass-transfer coefficient that depends exponentially on relative humidity or water activity. This resistance does not seem to exist for liquid/membrane or membrane/membrane interfaces. The effect of the interfacial resistance is to flatten the water-content profiles within the membrane during operation. Under typical operating conditions, the resistance is on par with the water-transport resistance of the bulk membrane. Thus, the interfacial resistance can be dominant especially in thin, dry membranes and can affect overall fuel-cell performance.

While the interfacial resistance has been quantified, there is still a need for further research. One avenue to be explored is the cause of the resistance. Throughout the discussion, there has been an underlying concept that the morphology is different at the membrane interface than within the bulk. Future work is aimed at quantifying this difference in terms of structural and chemical properties such as the amount of hydrophilic surface moieties as a function of relative humidity, some of which has been done in the literature, but not under all relevant conditions. Furthermore, while the impact of interfacial resistance on water-transport has been quantified, there is still a need for quantification and explanation of interfacial resistance to ions, gases, etc. Future work is also aimed at examining the impact of any interfacial effects in the catalyst-layer ionomer and the use of interfacial resistance at the catalyst-layer / membrane interface which can contain membrane, gas, and liquid interfaces. For example, for a macroscopic treatment, the interfacial resistance described in this paper can be averaged depending on the volume fraction of the requisite phases (in agreement with the idea of more hydrophilic surface area with humidity), although verification of such an approach is required. Finally, one can go back and review many of the membrane and PEFC modeling literature in the last few years and see if the conclusions remain valid with the addition of interfacial resistances.

Acknowledgements

This work was supported by CRADA agreement LB08003874 between LBNL and TMC as well as the Assistant Secretary for Energy Efficiency and Renewable Energy, Office of Hydrogen, Fuel Cell, and Infrastructure Technologies, of the U. S. Department of Energy under contract number DE-AC02-05CH11231.

References

[1] Weber, A. Z., and Newman, J., 2004, "Modeling Transport in Polymer-Electrolyte Fuel Cells," Chemical Reviews, 104(10), pp. 4679-4726.
[2] Zawodzinski Jr., T. A., Gottesfeld, S., Shoichet, S., and Mccarthy, T. J., 1993, "The Contact Angle between Water and the Surface of Perfluorosulphonic Acid Membranes," Journal of Applied Electrochemistry, 23(pp. 86-88.
[3] Van Nguyen, T., Nguyen, M. V., Nordheden, K. J., and He, W., 2007, "Effect of Bulk and Surface Treatments on the Surface Ionic Activity of Nafion Membranes," Journal of the Electrochemical Society, 154(11), pp. A1073-A1076.
[4] Mclean, R. S., Doyle, M., and Sauer, B. B., 2000, "High-Resolution Imaging of Ionic Domains and Crystal Morphology in Ionomers Using Afm Techniques," Macromolecules, 33(17), pp. 6541-6550.
[5] Aleksandrova, E., Hiesgen, R., Friedrich, K. A., and Roduner, E., 2007, "Electrochemical Atomic Force Microscopy Study of Proton Conductivity in a Nafion Membrane," Physical Chemistry Chemical Physics, 9(21), pp. 2735-2743.
[6] Takimoto, N., Wu, L., Ohira, A., Takeoka, Y., and Rikukawa, M., 2009, "Hydration Behavior of Perfluorinated and Hydrocarbon-Type Proton Exchange Membranes: Relationship between Morphology and Proton Conduction," Polymer, 50(2), pp. 534-540.
[7] Van Nguyen, T., Nguyen, M. V., Lin, G. Y., Rao, N. X., Xie, X., and Zhu, D. M., 2006, "Characterization of Surface Ionic Activity of Proton Conductive Membranes by Conductive Atomic Force Microscopy," Electrochemical and Solid State Letters, 9(2), pp. A88-A91.
[8] Bass, M., and Freger, V., 2008, "Hydration of Nafion and Dowex in Liquid and Vapor Environment: Schroeder's Paradox and Microstructure," Polymer, 49(2), pp. 497-506.
[9] Ge, S. H., Li, X. G., Yi, B. L., and Hsing, I. M., 2005, "Absorption, Desorption, and Transport of Water in Polymer Electrolyte Membranes for Fuel Cells," Journal of the Electrochemical Society, 152(6), pp. A1149-A1157.
[10] Monroe, C. W., Romero, T., Merida, W., and Eikerling, M., 2008, "A Vaporization-Exchange Model for Water Sorption and Flux in Nafion," Journal of Membrane Science, 324(1-2), pp. 1-6.
[11] Satterfield, M. B., and Benziger, J. B., 2008, "Non-Fickian Water Vapor Sorption Dynamics by Nafion Membranes," Journal of Physical Chemistry B, 112(12), pp. 3693-3704.
[12] Aotani, K., Miyazaki, S., Kubo, N., and Katsuta, M., 2008, "An Analysis of the Water Transport Porperties of Polymer Electrolyte Membrane," ECS Transactions, 16(2), pp. 341-352.
[13] Majsztrik, P. W., Satterfield, M. B., Bocarsly, A. B., and Benziger, J. B., 2007, "Water Sorption, Desorption and Transport in Nafion Membranes," Journal of Membrane Science, 301(1-2), pp. 93-106.
[14] Tsampas, M. N., Pikos, A., Brosda, S., Katsaounis, A., and Vayenas, C. G., 2006, "The Effect of Membrane Thickness on the Conductivity of Nafion," Electrochimica Acta, 51(13), pp. 2743-2755.
[15] Sethuraman, V. A., Khan, S., Jur, J. S., Haug, A. T., and Weidner, J. W., 2009, "Measuring Oxygen, Carbon Monoxide and Hydrogen Sulfide Diffusion Coefficient and Solubility in Nafion Membranes," Electrochimica Acta, pp. in press.
[16] Adachi, M., Navessin, T., Xie, Z., Frisken, B., and Holdcroft, S., 2009, "Correlation of in Situ and Ex Situ Measurements of Water Permeation through Nafion Nre211 Proton Exchange Membranes," Journal of the Electrochemical Society, 156(6), pp. B782-B790.
[17] Freger, V., 2009, "Hydration of Ionomers and Schroeder's Paradox in Nafion," Journal of Physical Chemistry B, 113(1), pp. 24-36.

[18] Goswami, S., Klaus, S., and Benziger, J., 2008, "Wetting and Absorption of Water Drops on Nafion Films," Langmuir, 24(16), pp. 8627-8633.
[19] Weber, A. Z., and Newman, J., 2004, "Transport in Polymer-Electrolyte Membranes. Ii. Mathematical Model," Journal of the Electrochemical Society, 151(2), pp. A311-A325.
[20] Motupally, S., Becker, A. J., and Weidner, J. W., 2000, "Diffusion of Water in Nafion 115 Membranes," Journal of the Electrochemical Society, 147(9), pp. 3171-3177.
[21] Tsushima, S., Teranishi, K., and Hirai, S., 2005, "Water Diffusion Measurement in Fuel-Cell Spe Membrane by Nmr," Energy, 30(2-4), pp. 235-245.
[22] Pivovar, A. A., and Pivovar, B. S., 2005, "Dynamic Behavior of Water within a Polymer Electrolyte Fuel Cell Membrane at Low Hydration Levels," Journal of Physical Chemistry B, 109(2), pp. 785-793.
[23] Zawodzinski, T. A., Derouin, C., Radzinski, S., Sherman, R. J., Smith, V. T., Springer, T. E., and Gottesfeld, S., 1993, "Water Uptake by and Transport through Nafion(R) 117 Membranes," Journal of the Electrochemical Society, 140(4), pp. 1041-1047.
[24] Weber, A. Z., and Newman, J., 2009, Device and Materials Modeling in Pem Fuel Cells, A Combination Model for Macroscopic Transport in Polymer-Electrolyte Membranes.
[25] Bernardi, D. M., and Verbrugge, M. W., 1992, "A Mathematical Model of the Solid-Polymer-Electrolyte Fuel Cell," Journal of the Electrochemical Society, 139(pp. 2477-2491.
[26] Meier, F., and Eigenberger, G., 2004, "Transport Parameters for the Modelling of Water Transport in Ionomer Membranes for Pem-Fuel Cells," Electrochimica Acta, 49(11), pp. 1731-1742.
[27] Aotani, K., Miyazaki, S., Kubo, N., and Katsuta, M., 2008, "An Analysis of the Water Transport Properties of
Polymer Electrolyte Membrane," ECS Transactions, 16(2), pp. 341-352.
[28] Majsztrik, P., Bocarsly, A. B., and Benziger, J., 2008, Journal of Physical Chemistry B, 112(pp. 16280.

Captions

Table I. Liquid-water permeability through Nafion 21x membranes as a function of cell temperature and thickness.

Table II. Water-flux data with small activity differences across Nafion 21x membranes.

Figure 1. Schematics of the experimental (a) liquid-water and (b) water-vapor permeation cells.

Figure 2. Water flux across a LE/VE cell with a Nafion® 212 membrane as a function of liquid-water pressure in the first chamber with gas streams having average water activities of 0.54, 0.70, and 0.85 in the second chamber at 80°C.

Figure 3. Resistance to water transport in Nafion 21x membranes as a function of membrane wet thickness for different activities.

Figure 4. Derived interfacial-resistance coefficient as a function of water activity.

Figure 5. Modeled water flux (lines) compared to experimental water-flux data (points) as a function of average water activity for three Nafion 21x membrane configurations.

Figure 6. Fraction of total resistance due to interfacial effects as a function of both membrane dry thickness and water activity.

Figure 7. Water concentration profiles for several representative cases. In all cases the water activity at length zero is set to 0.2. In LE/VE cases the LE side is at 1 bar water pressure with no interfacial resistance. For VE/VE cases, the high activity side is at

unit activity. I) LE/VE cell with high liquid water permeability. II) LE/VE cell with low liquid water permeability. III) VE/VE cell with no interfacial resistance. IV) VE/VE cell with interfacial resistance.

Figure 8. Water activity at the low-humidity side as a function of current density (going in the positive direction) across the membrane for positive, negative and zero net water fluxes for both simulations with (solid) and without (dotted) interfacial effects included.

Table I. Liquid-water permeability through Nafion 21x membranes as a function of cell temperature and thickness.

Sample	Temperature (°C)	Permeability ($x10^{-16}$ cm^2)
21x 211	25	1.09
21x 212	25	1.09
21x 212	60	5.57
21x 212	80	6.76

Table II. Water-flux data with small activity differences across Nafion 21x membranes.

Nafion	Wet (LE) thickness t μm	Water flux $\mathbf{N}$ μmol/cm^2/s	Average water activity a	Difference of water activity Δa	Normalized flux $\mathbf{N}t/\Delta a$ μmol/cm/s
211	27	16.9	0.85	0.058	0.785
	27	9.53	0.65	0.077	0.335
	27	4.74	0.45	0.092	0.139
	27	3.07	0.25	0.095	0.087
212	54	12.0	0.85	0.076	0.856
	54	5.35	0.65	0.086	0.335
	54	3.21	0.45	0.087	0.200
	54	1.66	0.25	0.092	0.098
211+212	81	9.43	0.85	0.080	0.954
	81	4.26	0.65	0.086	0.401
	81	2.22	0.45	0.094	0.192
	81	1.52	0.25	0.102	0.120

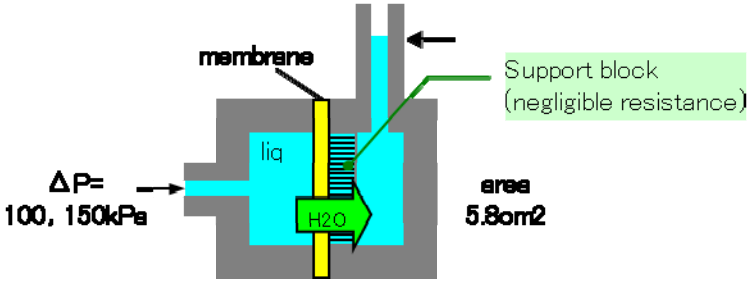

(a)

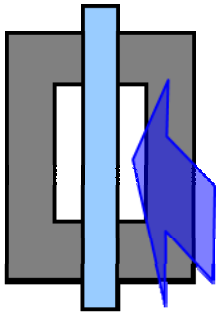

(b)

Figure 1. Schematics of the experimental (a) liquid-water and (b) water-vapor permeation cells.

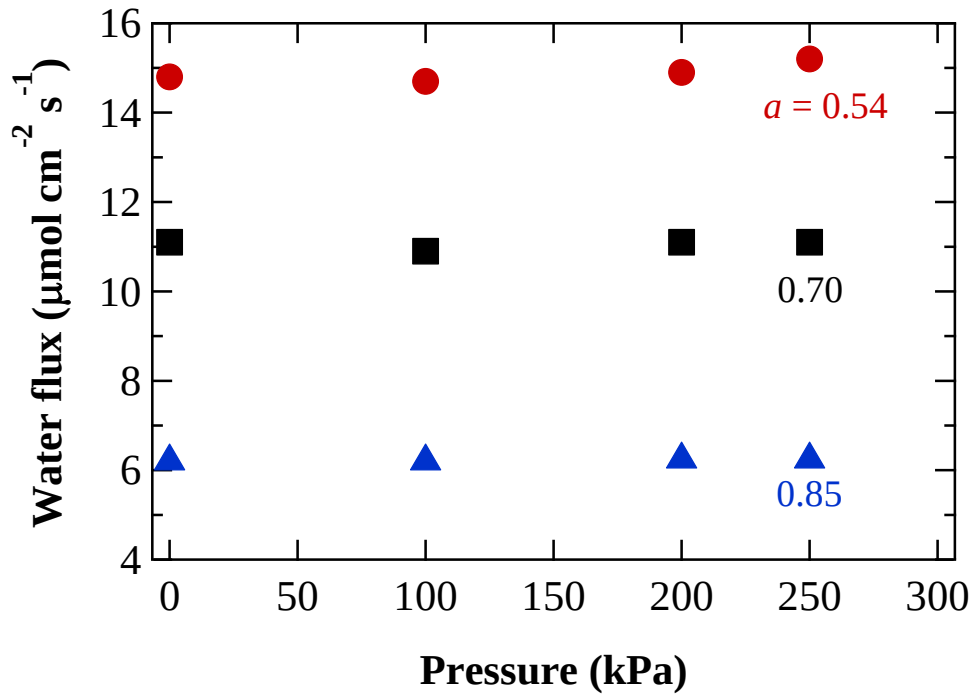

Figure 2. Water flux across a LE/VE cell with a Nafion® 212 membrane as a function of liquid-water pressure in the first chamber with gas streams having average water activities of 0.54, 0.70, and 0.85 in the second chamber at 80°C.

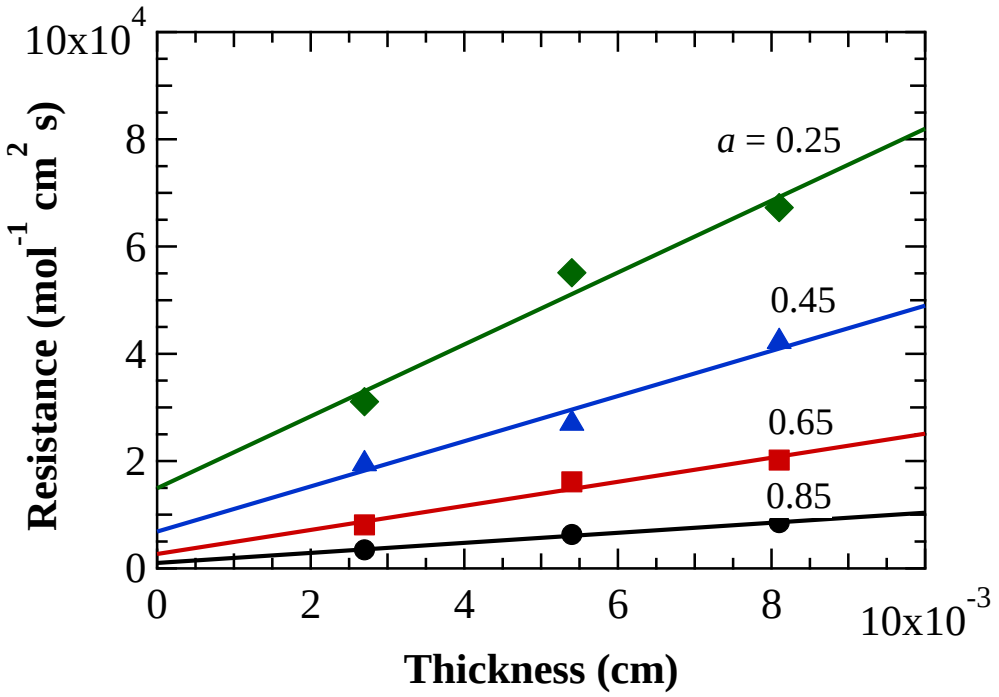

Figure 3. Resistance to water transport in Nafion 21x membranes as a function of membrane wet thickness for different activities.

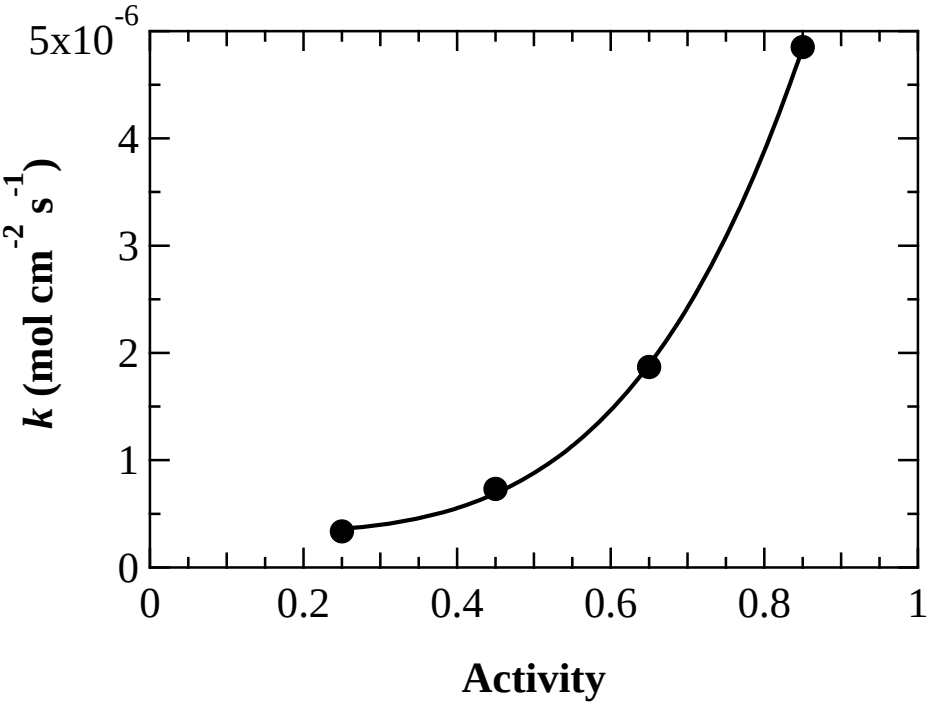

Figure 4. Derived interfacial-resistance coefficient as a function of water activity.

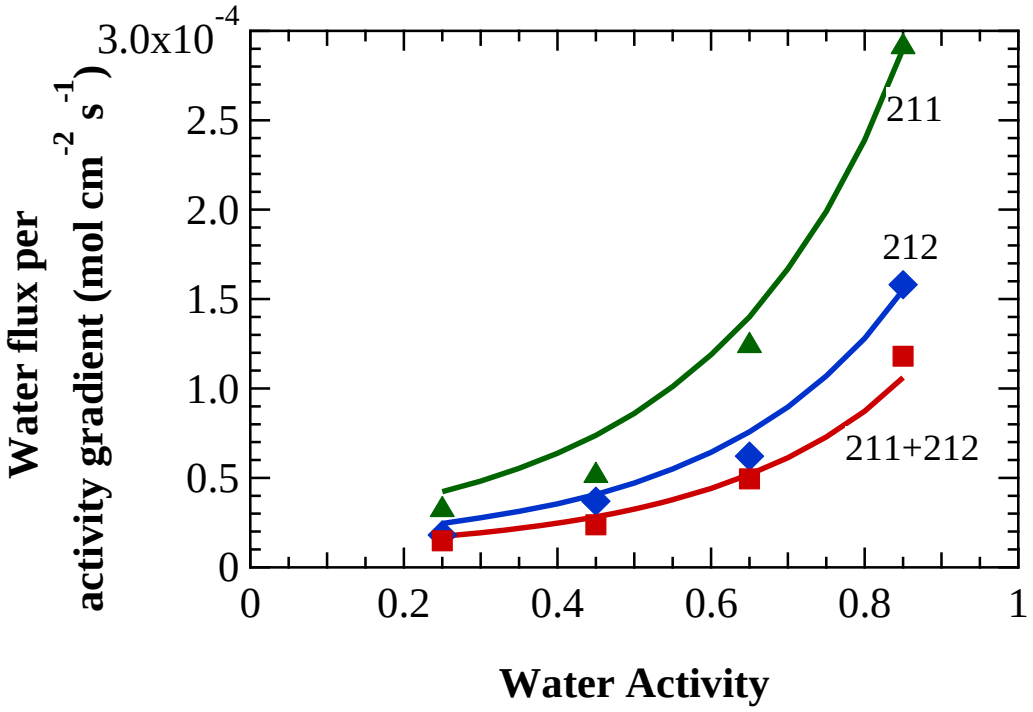

Figure 5. Modeled water flux (lines) compared to experimental water-flux data (points) as a function of average water activity for three Nafion 21x membrane configurations.

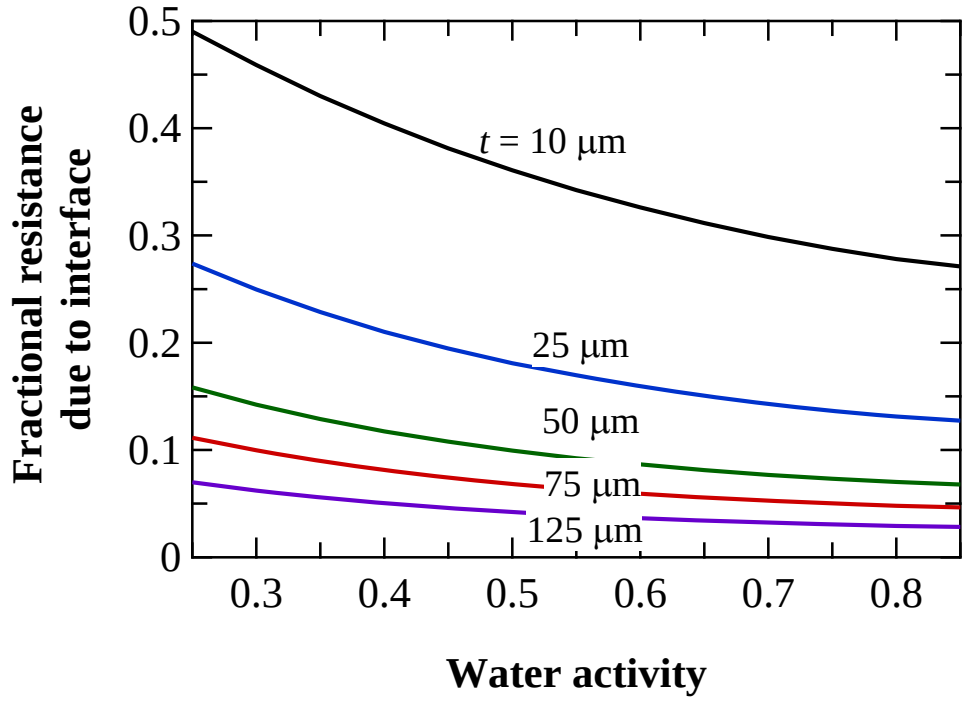

Figure 6. Fraction of total resistance due to interfacial effects as a function of both membrane dry thickness and water activity.

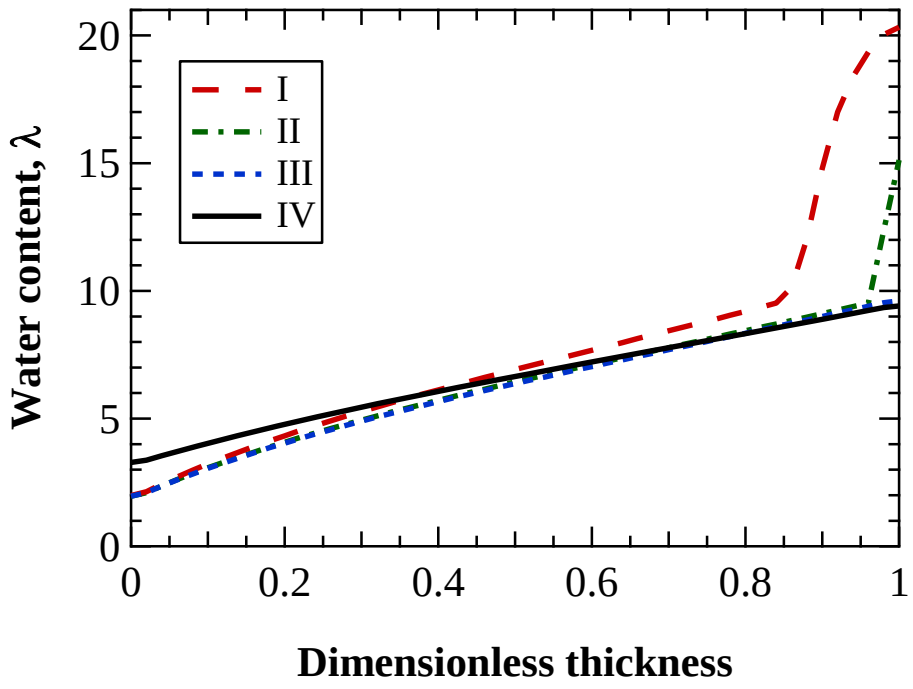

Figure 7. Water concentration profiles for several representative cases. In all cases the water activity at length zero is set to 0.2. In LE/VE cases the LE side is at 1 bar water pressure with no interfacial resistance. For VE/VE cases, the high activity side is at unit activity. I) LE/VE cell with high liquid water permeability. II) LE/VE cell with low liquid water permeability. III) VE/VE cell with no interfacial resistance. IV) VE/VE cell with interfacial resistance.

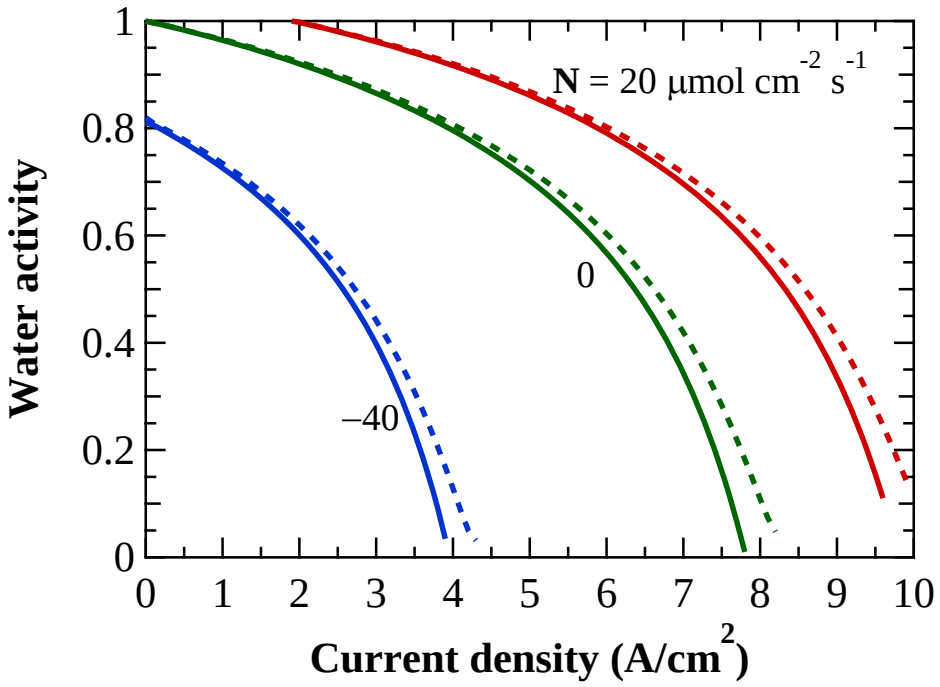

Figure 8. Water activity at the low-humidity side as a function of current density (going in the positive direction) across the membrane for positive, negative and zero net water fluxes for both simulations with (solid) and without (dotted) interfacial effects included.